

Spectroscopic evidence of Kondo-induced quasi-quartet in CeRh₂As₂

Denise S. Christovam,¹ Miguel Ferreira-Carvalho,^{1,2} Andrea Marino,¹ Martin Sundermann,^{3,1}

Daisuke Takegami,¹ Anna Melendez-Sans,¹ Ku Ding Tsuei,⁴ Zhiwei Hu,¹ Sahana Rößler,¹ Manuel Valvidares,⁵ Maurits W. Haverkort,⁶ Yu Liu,^{7,*} Eric D. Bauer,⁷ Liu Hao Tjeng,¹ Gertrud Zwicky,^{8,1} and Andrea Severing^{2,1}

¹Max Planck Institute for Chemical Physics of Solids, Nöthnitzer Str. 40, 01187 Dresden, Germany

²Institute of Physics II, University of Cologne, Zùlpicher Str. 77, 50937 Cologne, Germany

³PETRA III, Deutsches Elektronen-Synchrotron DESY, Notkestraße 85, 22607 Hamburg, Germany

⁴National Synchrotron Radiation Research Center, 101 Hsin-Ann Road, Hsinchu 30077, Taiwan

⁵ALBA Synchrotron Light Source, Cerdanyola del Valles, Barcelona 08290, Spain

⁶Institute for Theoretical Physics, Heidelberg University, Philosophenweg 19, 69120 Heidelberg, Germany

⁷Los Alamos National Laboratory, Los Alamos, New Mexico 87545, USA

⁸Technische Universität Braunschweig, Braunschweig, Germany

(Dated: January 24, 2024)

CeRh₂As₂ is a new multiphase superconductor with strong suggestions for an additional itinerant multipolar ordered phase. The modeling of the low temperature properties of this heavy fermion compound requires a quartet Ce³⁺ crystal-field ground state. Here we provide the evidence for the formation of such a quartet state using x-ray spectroscopy. Core-level photoelectron and x-ray absorption spectroscopy confirm the presence of Kondo hybridization in CeRh₂As₂. The temperature dependence of the linear dichroism unambiguously reveals the impact of Kondo physics for coupling the Kramer's doublets into an effective quasi-quartet. Non-resonant inelastic x-ray scattering data find that the $|\Gamma_7^- \rangle$ state with its lobes along the 110 direction of the tetragonal structure (xy orientation) contributes most to the multi-orbital ground state of CeRh₂As₂.

Characterizing novel ordering and understanding how they arise is key for the development of functional materials. Heavy-fermion materials have been important model systems for the discovery of novel phases as well as their cooperation, coexistence, or competition. This is due to the fact that the characteristic energy scale of these materials is of the order of a few meV which, in turn, implies a high tunability of the electronic properties [1–5]. CeRh₂As₂ is a heavy-fermion system of high current interest, experimentally [6–11] as well as theoretically [12–21]. This material exhibits multiphase unconventional superconductivity (SC) [22, 23] and putative itinerant multipolar order; there are indications for a quadrupolar density wave (QDW) below $T_0 = 0.48$ K and above the superconducting transition at $T_{SC} \approx 0.31$ K; the transition temperatures refer to newer sample generations [24]. The unusual behavior of CeRh₂As₂ is due to the presence of $4f$ electrons. This conclusion is derived from the properties of its non- f reference compound LaRh₂As₂ that can be quantitatively described by standard Eliashberg theory of strong-coupling electron-phonon superconductors [25]. For understanding the low temperature (T) phases of CeRh₂As₂ it is also crucial that its f electrons form a quasi-quartet ground state.

In the heavy fermion state, the $4f$ degrees of freedom form heavy quasiparticles due to the Kondo effect (cf -hybridization). CeRh₂As₂ forms in the globally centro-symmetric tetragonal CaBe₂Ge₂ structure with two identical Ce sites per unit cell. The Ce sites lack

inversion symmetry so that the local point symmetry is C_{4v} but the crystal-field split Ce³⁺ Hund's rule ground state of Ce³⁺ may be treated like D_{4h} because the contribution of $5d$ states is negligible. Accordingly, the three Kramer's doublets can be written in J_z formalism as $|\Gamma_7^- \rangle = \sqrt{1 - \alpha^2} \cdot |\pm 3/2 \rangle - |\alpha| \cdot |\mp 5/2 \rangle$, $|\Gamma_6 \rangle = |\pm 1/2 \rangle$, $|\Gamma_7^+ \rangle = \sqrt{1 - \alpha^2} \cdot |\pm 5/2 \rangle + |\alpha| \cdot |\mp 3/2 \rangle$, and the f contribution to the quasi-particles has the character of the crystal-field ground state when the excited states are well separated from the ground state. However, if the system presents a Kondo temperature T_K of the order of magnitude of crystal-field splittings energies Δ_i , one may expect the Kondo effect to induce an effective quasi-quartet ground state. Its character reflects both states of the quasi-quartet.

The conjecture of a Kondo induced quasi-quartet is at the heart of renormalized band structure calculations in Ref. [9] that find superconductivity and other types of order may exist at different sites of the Fermi surface. Here, we investigate the electronic structure of Ce in CeRh₂As₂ in order to find spectroscopic evidence for such a quasi-quartet. Core-level photoelectron spectroscopy with hard x-rays (HAXPES) is sensitive to covalence and hence to the filling n_f of the Ce $4f$ shell [26–29]. Also x-ray absorption spectroscopy (XAS) at the Ce $M_{4,5}$ edges can reveal signatures of hybridization effects by exhibiting, in addition to the main transition $3d^{10}4f^1 \rightarrow 3d^9 4f^2$, a satellite induced by hybridization with the $3d^{10}4f^0$ configuration [26, 27, 30]. The linear dichroism (LD) of XAS at the Ce $M_{4,5}$ edges, on the other hand, is sensitive to the symmetry of the crystal-field ground state when exploiting the dipole selection rules of linear polarized light [30, 31]; at low T the ground state is probed and excited states contribute to the net dichroism

* Center for Correlated Matter and Department of Physics, Zhejiang University, Hangzhou 310058, China

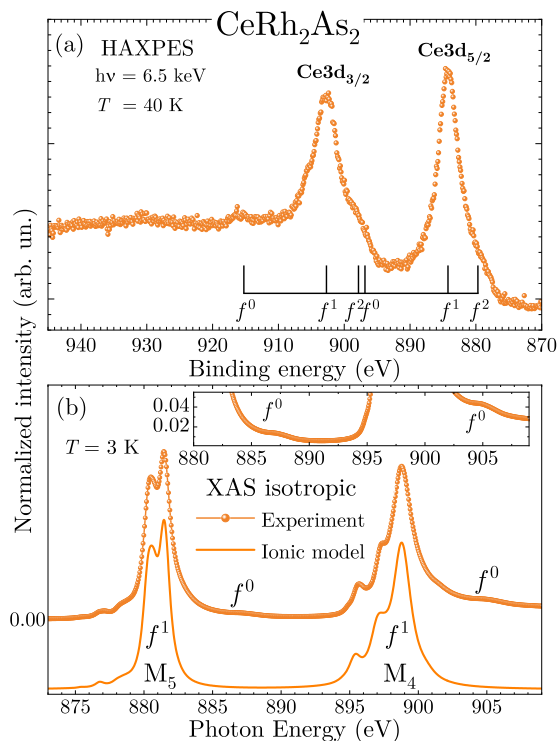


FIG. 1. (a) Ce 3d core level HAXPES data of CeRh₂As₂. The black ruler at the bottom indicates the position of the f^0 , f^1 and f^2 spectral weights. (b) Isotropic XAS spectrum of CeRh₂As₂ (dots) and the corresponding ionic multiplet simulation of the f^1 configuration (solid line). The inset shows a close-up to the energy regions with the f^0 satellites.

when they are populated thermally. This way the T -dependence of the LD provides insight into the sequence of crystal-field states, and size of the crystal-field splitting energies $\Delta_{1,2}$. Non-resonant inelastic x-ray scattering (NIXS) is also sensitive to the crystal-field ground state but it is based on multipole selection rules [32–36]. In NIXS, the direction of the momentum transfer with respect to the sample orientation takes over the role of the electric field vector in XAS. In contrast to XAS, NIXS is also sensitive to anisotropies with fourfold rotational symmetry, so that the orientation of e.g. a $|\Gamma_7^{+/-}\rangle$ charge density within the tetragonal unit cell can be determined.

In the present letter, we report results of HAXPES as well as XAS and NIXS measurements of CeRh₂As₂ single crystals. The spectra are analyzed with a full multiplet calculation to gain insight into the electronic structure of the crystal-field split Hund’s rule ground state of Ce³⁺. We use a simplified Anderson impurity calculation (SIAM) in the non-crossing approximation (NCA) to show that in the presence of the Kondo effect and in case $T_K \approx \Delta_i$, the excited crystal-field states do contribute to the LD also at low temperatures.

Growth and characterization of single crystalline CeRh₂As₂ are described in the Appendix. The transition temperatures are $T_{SC} = 0.30$ K and $T_0 = 0.45$ K, which is in very good agreement with the values reported for

newer generations of samples [24].

XAS spectra at the Ce $M_{4,5}$ edges (880-904 eV) were measured in the total electron yield mode (TEY) at beamline BL29 BOREAS at ALBA synchrotron, Spain [37] with an energy resolution of 300 meV. Clean sample surfaces were obtained by cleaving the CeRh₂As₂ single crystals *in-situ* in an ultra-high-vacuum (UHV) of about 1×10^{-9} mbar prior to inserting them into the main chamber with a base pressure of 10^{-10} mbar. XAS data were taken at 3, 50, 100, and 200 K with the electric field $\vec{E} \parallel ab$ and $\vec{E} \parallel c$. NIXS experiments were performed at the Max-Planck NIXS end station P01 at PETRA III/DESY, Germany at 8 K with the same set-up as described in Ref. [38]. The average momentum transfer amounted to $|\vec{q}| = 9.6 \pm 0.1 \text{ \AA}^{-1}$. The $N_{4,5}$ edges were measured with the momentum transfer \vec{q} parallel to [100], to [110], and [001]. HAXPES experiments were carried out at the Max-Planck-NSRRC HAXPES end station at the Taiwan undulator beam line BL12XU at SPring-8, Japan with a photon energy of about 6.5 keV, an overall energy resolution of 250 meV, and a sample temperature of 40 K [39]. Samples were polished *in-situ* in order to expose a fresh layer, and wide-scans were performed to ensure the absence of O and C 1s signal from surface contamination or oxidation. The pressure in the main chamber was in the low 10^{-10} mbar. More information about the experimental set-ups can be found in the Appendix.

XAS and NIXS data are simulated with the full multiplet code *Quanty* [40], starting with atomic parameters from the Cowan code [41], and applying typical reductions for the respective Hartree-Fock values of the Slater integrals and spin orbit values [42] (see Appendix). The reduction factors were optimized to best reproduce the isotropic spectrum in the case of XAS [31] and (pseudo)isotropic for NIXS. Both are constructed from the directional dependent data ($I_{iso} = (2I_{\parallel ab} + I_{\parallel c})/3$). Furthermore, a Gaussian and Lorentzian broadening are applied to account for resolution and lifetime effects (see Appendix).

Figure 1(a) shows the Ce 3d core level HAXPES data of CeRh₂As₂ without any background correction. CeRh₂As₂ shows the three spectral weights that arise in the presence of the core hole, when the ground state is a coherent interference of the $4f^0$, $4f^1$, and $4f^2$ configurations [28]. Also the *isotropic* XAS spectrum, shown in Fig 1 (b), reveals the presence of a $4f$ configuration different from $4f^1$. The spectral weights corresponding to the $3d^{10}4f^0 \rightarrow 3d^94f^1$ transition show up as small satellites on the high energy tails of the M_5 and M_4 absorption lines, shown on an enlarged scale in the inset. These small intensities originating from the $4f^0$ configuration confirm that the Kondo effect is indeed present in CeRh₂As₂, an aspect that turns out to be crucial for the analysis of the temperature dependence of the linear dichroism in the XAS spectra as discussed below.

The top spectra of Fig.2 show the polarization

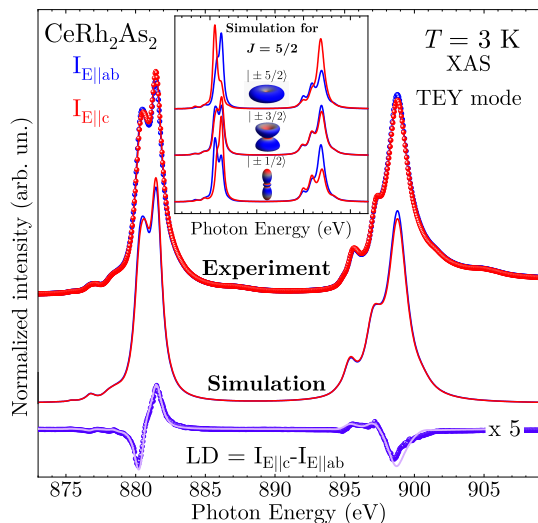


FIG. 2. Linear polarized XAS spectra of CeRh_2As_2 at 3 K for the electric field vector $\vec{E} \parallel c$ (red) and $\vec{E} \parallel ab$ plane (blue), and linear dichroism (purple), dots for the experiment and lines are the full multiplet simulation of the f^1 configuration. The inset shows the calculated individual contributions to each pure $|\pm J_z\rangle$ state.

dependent XAS data of CeRh_2As_2 at 3 K (red and blue circles) and at the bottom the experimental linear dichroism $\text{LD} = I_{E||c} - I_{E||ab}$ 5 times enlarged (purple circles). At first, we compare the data with the simulations of the pure $|\pm J_z\rangle$ states of the f^1 configuration that are displayed in the inset. Obviously a pure $|\pm 5/2\rangle$ and $|\pm 1/2\rangle$ can be excluded as ground state. The pure $|\pm 3/2\rangle$ may resemble the data best, but as we will explain below, we will need not only to consider the correct crystal-field scheme but also the Kondo effect. We note that the measured dichroic signal is relatively small and we verify its reliability by analyzing the lineshape. We recall that the lineshape of the $M_{4,5}$ dichroism of Ce^{3+} ions is unique as long as the crystal-field splitting is negligible compared to the inverse lifetime of the $M_{4,5}$ white lines, see Ref.s [43, 44]. After optimizing the reduction factors by means of the isotropic spectrum (see Fig.1(b)), we plot this unique lineshape on top of the measured dichroic spectrum and we indeed conclude that the experimental features all belong to a Ce^{3+} ion in the small crystal-field limit. Also the corresponding simulations for the $M_{4,5}$ spectra match the measured ones excellently.

The temperature dependence of the $\text{LD}(T)$ at the M_5 and M_4 edges is shown on an expanded energy scale in Fig. 3(a) for 3, 50, 100, and 200 K. The LD at 50 K has increased with respect to 3 K, as indicated by the arrows. The change in $\text{LD}(T)$ indicates that an excited crystal-field state is close. $\text{LD}(T)$ remains almost as large at 100 K, and then decreases when warming up to 200 K. Also here it is informative to understand the T -dependence of the LD by looking at first at the pure $|\pm J_z\rangle$ states that are depicted in the inset of Fig.2. The $|\pm 1/2\rangle$ has a stronger dichroism of the same sign as the one at 3 K

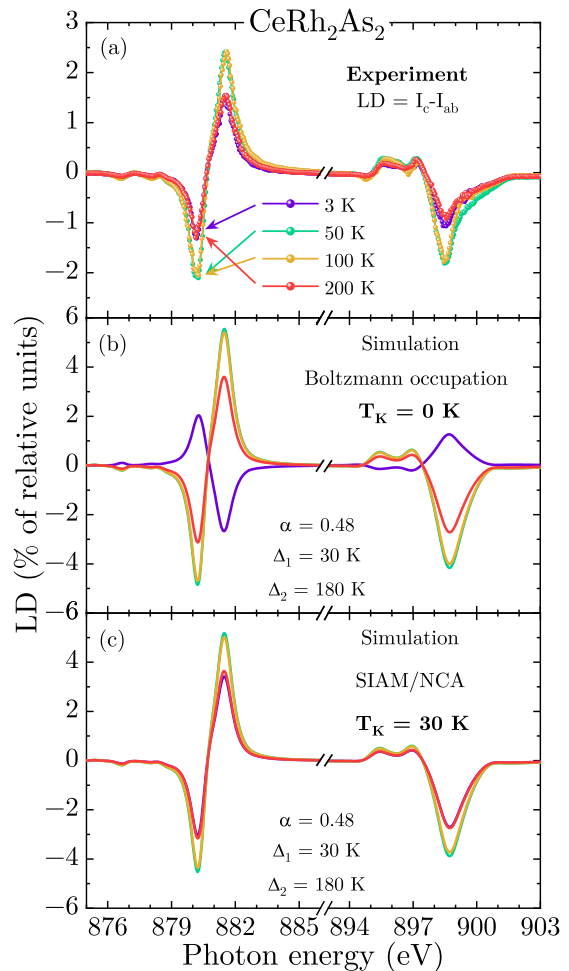


FIG. 3. (a) Measured T -dependence of the LD at $T=3$ (purple), 50 (green), 100 (yellow), and 200 K (red). The panels below show two different simulations, an ionic crystal-field calculation considering the Boltzmann occupation of excited states but no Kondo effect (b), and the same crystal-field model including the Kondo effect (c), see text. The scale was multiplied by 100 to show the percentage of LD.

whereas the LD of the $|\pm 5/2\rangle$ state is large and opposite. Hence, the increase of the $\text{LD}(T)$ when warming up to 50 K must be due to the increasing population of the $|\Gamma_6\rangle = |\pm 1/2\rangle$ state, followed by the successive population of the second $|\Gamma_7^{-/+}\rangle$ state of majority $|\pm 5/2\rangle$ that compensates the LD of the $|\Gamma_6\rangle$ when warming up further to 100 and 200 K.

First, we simulate $\text{LD}(T)$ by assuming the crystal-field model that satisfies the macroscopic data best, especially the high temperature anisotropy of the static susceptibility where the impact of the Kondo effect can be neglected. Hafner *et al.*[9] propose the sequence of states that we obtain from the above comparison with the pure $|J_z\rangle$ states, with $\Delta_1=30$ K, $\Delta_2=180$ K and $\alpha=0.48$ for the crystal-field splittings and mixing factor of the ground state, respectively. These numbers are based on the analysis of the specific heat and static susceptibility. This model reproduces qualitatively

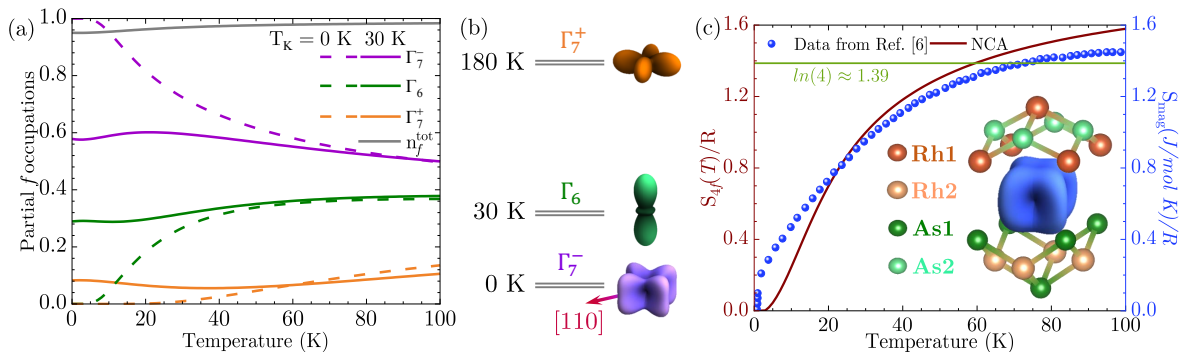


FIG. 4. (a) SIAM/NCA calculation of partial $4f$ occupations for $T_K = 30$ K (solid lines) and Boltzmann statistics ($T_K = 0$ - dashed lines) for the crystal-field scheme according Ref.[9], shown in (b), with $|\Gamma_7^- \rangle = 0.88 | \pm 3/2 \rangle - 0.48 | \mp 5/2 \rangle$, $|\Gamma_6 \rangle = | \pm 1/2 \rangle$, $|\Gamma_7^+ \rangle = 0.88 | \pm 5/2 \rangle + 0.48 | \mp 3/2 \rangle$. (c) SIAM/NCA calculated entropy as function of temperature (red solid line) compared to specific heat data from Ref. [6] (blue dots) and expected entropy of a quartet (horizontal green line). Inset: Ce charge density of the Kondo-mixed ground state (58% $|\Gamma_7^- \rangle$, 29% $|\Gamma_6 \rangle$, and 8% $|\Gamma_7^+ \rangle$) with its nearest neighbors.

LD(T) at 50, 100, and 200 K when taking into account the respective Boltzmann occupations of the excited states (see Fig.3(b)). It contradicts, however, the experiment at low temperatures where the Kondo effect starts to manifest: at 3 K the simulated LD turns out to be opposite to the experimental one (compare Fig.3(a) and (b)).

We take the discrepancy between data and crystal-field simulation of LD(T) at low T as a strong suggestion for having to consider the impact of the Kondo interaction since Kondo is a low T effect. The SIAM/NCA calculations [44–46] take into account the hybridization of the three crystal-field states with the conduction electron bath. It turns out that the Kondo effect induces a finite occupation of the first and second excited crystal-field states also at 3 K, in contrast to the Boltzmann occupations where only the lowest state is occupied. The Kondo induced (solid lines) and Boltzmann-only (dashed lines) occupations as function of T are displayed in Fig.4(a). The SIAM/NCA calculations take into account the same crystal-field model as above and a Kondo temperature T_K of 30 K. The latter is suggested from macroscopic data [6, 9]. The Kondo-mixed ground state at low T is calculated with a $4f$ -shell occupation of $n_f^{tot} = 95\%$. Beginning at 50 K, but certainly at 100 K the differences between Kondo induced and Boltzmann-only occupation are negligible. Therefore, the Kondo effect has the strongest impact on the simulated LD(T) at 3 K: due to the Kondo induced contribution of the higher lying states, the sign of the LD at 3 K is now correctly reproduced (see Fig.3(c)).

The calculation of the entropy within the SIAM/NCA model based on the above crystal-field scheme and Kondo temperature yields the red line in Fig.4(c), which reproduces $R \ln 4$ at about 60 K very well, and it is in good agreement with the analysis of the experimental specific heat (blue dots) by Khim *et al.* [6].

While a T_K of 30 K reproduces LD(T) well, we show in the Appendix analyses with other T_K values. We find that a lower value of $T_K = 15$ K still produces the

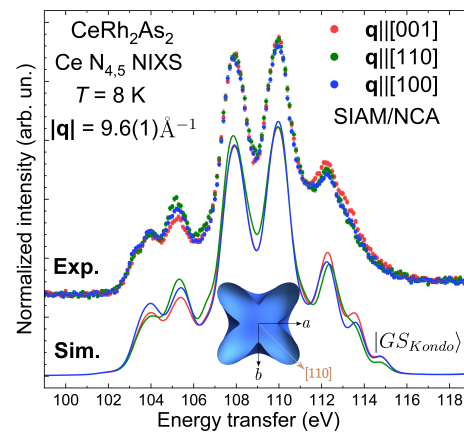


FIG. 5. Normalized and background corrected NIXS data for $\mathbf{q} \parallel [001]$ (red), $\mathbf{q} \parallel [110]$ (green) and $\mathbf{q} \parallel [100]$ (blue). The lines represent the simulation in the SIAM/NCA work-frame for $|GS_{Kondo}\rangle$ ground state, with the $|\Gamma_7^- \rangle$ most strongly occupied. The inset represent the respective orbital orientation within the ab -plane.

wrong sign in the LD at 3 K, see Fig.6]. This indicates that $k_B T_K$ must be at least of the same order of magnitude as the crystal-field splitting, thus implying that the degeneracy of the relevant low-energy subspace is effectively higher than two-fold. We also find that the entropy sets limits on the upper and lower value of T_K , see Fig.7.

LD(T) is well described with a $|\Gamma_7^{\pm} \rangle$ lowest in energy. It is, however, not yet clear whether it is the $|\Gamma_7^+ \rangle$ ($x^2 - y^2$) or the $|\Gamma_7^- \rangle$ (xy orientation). We address this question with directional dependent NIXS. NIXS spectra at 8 K for momentum transfers $\vec{q} \parallel (100)$, $\vec{q} \parallel (110)$, and for completeness also for $\vec{q} \parallel (001)$, are displayed in Fig.5. The spectra are normalized to the integral of the Compton background at higher energy transfers, and a linear background is subtracted as described in the Appendix and displayed in Fig.8. The directional dependence in the ab -plane is fairly weak, except for a more distinct region at around 105 eV energy transfer.

The in-plane directional dependence gives the desired information about the sign of the $|\Gamma_7^{+/-}\rangle$ state. The 45° rotation would imply a switch in intensity of the (100)(blue) and (110)(green) signals. Also the NIXS spectra were simulated with the Kondo mixed ground state $|GS_{Kondo}\rangle$, using the respective occupations at 8 K. The Kondo mixing of states reduces and alters slightly the directional dependence in the ab -plane with respect to pure $|\Gamma_7^{+/-}\rangle$ states (see Fig. 8 in the Appendix) due to the admixture of the rotational invariant $|\Gamma_6\rangle$ and the excited $|\Gamma_7^{-/+}\rangle$ state with lobes rotated by 45° and, consequently, an opposite in-plane anisotropy. The resulting NIXS simulation with the orbital mixed ground state $|GS_{Kondo}\rangle$ shows that the lobes are along (110), thus confirming the $|\Gamma_7^- \rangle$ state must be the one most strongly occupied. A more detailed discussion about the NIXS spectra is found in the Appendix.

Putting together the results of macroscopic data, and the present T dependent XAS and low T NIXS, we find that the $4f^1$ part of the multi-orbital ground state wave function with $n_f^{tot}=0.95$ consists of $\sqrt{0.58}|\Gamma_7^- \rangle$, $\sqrt{0.29}|\Gamma_6\rangle$, and $\sqrt{0.08}|\Gamma_7^+ \rangle$ with $|\Gamma_7^- \rangle = 0.88|\pm 3/2\rangle - 0.48|\mp 5/2\rangle$, $|\Gamma_7^+ \rangle = 0.48|\pm 3/2\rangle + 0.88|\mp 5/2\rangle$, and $|\Gamma_6\rangle = |\pm 1/2\rangle$. The corresponding charge density is displayed in Fig. 4 (b) and Fig. 5. The dominance of the $|\Gamma_7^- \rangle$ state accommodates very well the Fermi surface as calculated in Ref. [9].

Quantitatively, the present simulation overestimates the T -dependence of $LD(T)$. This is most likely due to the fact that the present SIAM/NCA model is too simplistic. For example, the calculations performed on the NCA frame are in the limit $U \rightarrow \infty$, meaning they do not take into account the influence of the $4f^2$ configuration and all weight is concentrated on $4f^1$. Moreover, symmetry dependent hybridization is not taken into account, although renormalized band structure calculations that do consider symmetries [47] show that the $|\Gamma_7^+ \rangle$ at 180 K contributes significantly to the Fermi surface; actually more than expected from an isotropic calculation (see Fig. 10 in the Appendix).

To summarize, the presence of significant cf -hybridization in $CeRh_2As_2$ is consistent with core level HAXPES and M -edge XAS data. The temperature dependence of the linear dichroism $LD(T)$ in M -edge XAS is qualitatively reproduced with the crystal-field model that was suggested from the anisotropy of the static susceptibility and the specific heat when taking into account the Kondo induced coupling of all crystal-field states to the conduction electron bath. The resulting multi-orbital ground state is an effective quartet that reproduces well the asymptotic value of entropy from the specific heat, thus validating the conjecture of a quasi-quartet ground state that is crucial for superconductivity to coexist with other types of order.

I. ACKNOWLEDGEMENT

All authors thank Manuel Brando, Elena Hassinger, Javier Landaeta, and Konstantin Semeniuk for enlightening discussions. Katharina Höfer's expertise in designing the cleaving setup was extremely helpful and is appreciated by all authors. A.S and M. F.-C. benefited from support of the German Research Foundation (DFG), Project No. 387555779. Y. L. and E.D.B. were supported by the U.S. Department of Energy (DOE), Office of Basic Energy Sciences, Division of Materials Science and Engineering under project "Quantum Fluctuations in Narrow-Band Systems". XAS and XLD measurements were performed at ALBA under proposal ID 2022097004. We acknowledge DESY (Hamburg, Germany), a member of the Helmholtz Association HGF, for the provision of experimental facilities.

II. APPENDIX

A. Sample growth and characterization

Single crystals of $CeRh_2As_2$ were grown in Bi flux starting from a mixture of pure elements Ce, Rh, As, and Bi with a molar ratio of 1 : 2 : 2 : 30. The starting materials were sealed in an evacuated fused silica tube, which was heated to 1150°C over 30 h, followed by a dwell at 1150°C for 24 h. A *sawtooth* heating/cooling profile was used to produce larger and higher-purity crystals consisting of: cooling from 1150°C to 750°C at a rate of 20°C/hr. , heating to 1050°C at 75°C/hr. , cooling to 750°C at 7.5°C/hr. , heating to 1050°C at 75°C/hr. , then slowly cooling to 700°C at 1.9°C/hr.

The T_{SC} and T_0 of 0.30 and 0.45 K are in excellent agreement with the higher quality $CeRh_2As_2$ crystals from Semeniuk *et al.* [24]. The peak height and sharpness of the transition at T_{SC} and T_0 in the specific heat, and a residual resistivity of $RRR=2.4$, are all indications of improved crystal quality—all comparable to the Semeniuk samples.

The morphology of the $CeRh_2As_2$ single crystals was very well defined, presenting as thin platelets with the [001] direction normal to the plane, and their in-plane axes typically aligned to natural edges of the crystals.

B. Experimental details

The single-crystalline samples were aligned using the Laue method, and mounted according to the requirements of each technique. For cleaving the small crystals in the XAS experiments, minute grooves were machined into the sample holders where the crystals were glued, to provide more support to the stress of cleaving. Similarly, small custom-made posts were developed with a recess to fit into each sample and assure better grip. These precautions were needed because it turned out

that the crystals were very hard to cleave. The single-crystalline samples were aligned so that a surface with a [100] normal vector was exposed to the beam. This way, both polarizations, $\vec{E} \parallel ab$ and $\vec{E} \parallel c$, could be measured without rotating the sample. For NIXS the samples were mounted making use of the flat and mirror-like surfaces after aligned properly, so that the momentum transfers \vec{q} parallel to [100], to [110], and [001] could be realized. In the HAXPES experiment the photons are horizontally polarized. The MB Scientific A-1 HE analyzer was mounted horizontally at 90° [39], and the sample was measured with the [001] direction 15° away from the analyzer (near normal emission).

C. Simulations

The reduction of the atomic parameters accounts for configuration interaction effects that are not included in the Hartree-Fock scheme [42]. For the XAS simulations, the $4f$ - $4f$ and $3d$ - $4f$ Slater integrals, and the atomic value for the $3d$ spin-orbit were reduced by 39.0(5)% 17.5(5)%, and 2.7(5)%, respectively [31]. The reduction factors were optimized to best reproduce the isotropic spectrum that was constructed from the directional dependent data ($I_{iso} = (2I_{\parallel ab} + I_{\parallel c})/3$). A Gaussian broadening for resolution and an energy dependent Lorentzian broadening for life time effects was used.

For the NIXS simulations the resolution Gaussian shaped broadening of 0.7 eV and an additional Lorentzian broadening of 0.17 eV FWHM for life-time effects were taken into account. Here the Slater integrals for the $4f$ - $4f$ and $4d$ - $4f$ Coulomb interactions were reduced by about 26(1)% and 22(1)%, respectively. The spin-orbit reduction associated to the $4d$ was reduced by 2(1)%, and in particular, the Coulomb exchange term G^1 , that controls the dipolar contribution's energy transfer, was reduced by 35.5(5)%. Also here the reduction factors were optimized by reproducing the energy distribution of the (pseudo)isotropic Ce $N_{4,5}$ data that were, as for XAS, constructed from the directional dependent spectra.

D. Orbital occupation, LD(T) and entropy for different values of T_K

The contribution of excited crystal-field states to the orbital mixed ground state depends on the Kondo temperature. With increasing T_K , this contribution rises (see Fig. 6 (a)-(c)). For $T_K = 15$ K, the calculated linear dichroism (LD) in the 3 K XAS spectrum still has the wrong sign (see Fig. 6(d)), thus giving a lower limit for T_K . For $T_K = 60$ K the overall T -dependence is similar to the one of $T_K = 30$ K, but there is a general decrease of the LD signal (see Fig. 6(f)) which can be expected since in the limit that $k_B T_K$ is much larger than the crystal field splitting the LD will eventually become zero with no T -dependence, thereby reflecting

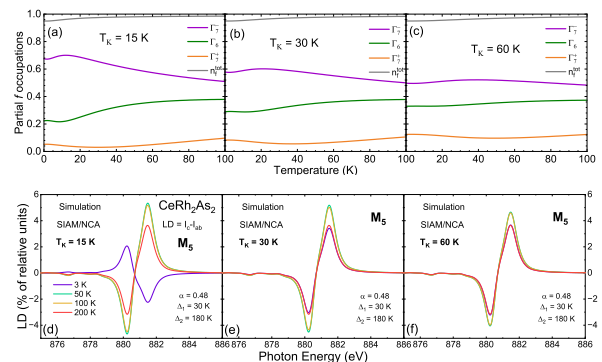


FIG. 6. (a)-(c) Partial occupation of f states according to SIAM/NCA calculation and (d)-(f) resulting LD(T) for $T_K = 15, 30, \text{ and } 60$ K.

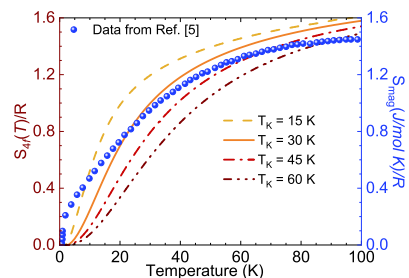


FIG. 7. Entropy calculated with SIAM/NCA for different values of T_K compared to the data from entropy from Ref. [6].

the spherically symmetric sixfold degenerate Hund's rule ground state. Fig. 7 shows the calculated entropy within the SIAM/NCA formalism for different values of T_K .

E. NIXS

Fig. 8 (a) shows the NIXS data of CeRh_2As_2 in a wide energy range showing the strong elastic signal at zero energy transfer, the Compton signal and the $n = 4$ intrashell core hole excitations, namely $N_{4,5}$ ($d \rightarrow f$), $N_{2,3}$ ($p \rightarrow f$) and N_1 ($s \rightarrow f$), the most intense and structured being the $N_{4,5}$. To normalize and average different scans, we fix an integration range over the Compton scattering and normalize to its area. Further, to treat the inclined background beneath the edge of interest, we overlay the detailed edge scan to a wide Compton scan measured immediately before or after. We then subtract a linear background considering the pre-edge and a reasonably far energy transfer above edge to avoid capturing post-edge effects (generally related to the detailed electronic structure of the material). The energy alignment process is described in detail in Ref. [48].

Fig. 8 (b) shows the constructed (pseudo)isotropic NIXS spectra at the Ce $N_{4,5}$ -edge and the simulation resulting from optimizing the reduction factors of the Slater integrals and the magnitude of \vec{q} . We increase

$|\vec{q}|$ to account for the extended radial wave function in the solid with respect to the atomic model. In particular, the reduction of the G^1 Slater integral tunes the position of the dipolar contribution, so we select its value based on aligning the (under-broadened) dipole excitation to the broad bump around 122 eV. In total the reduction factors agree well with previous analysis [36].

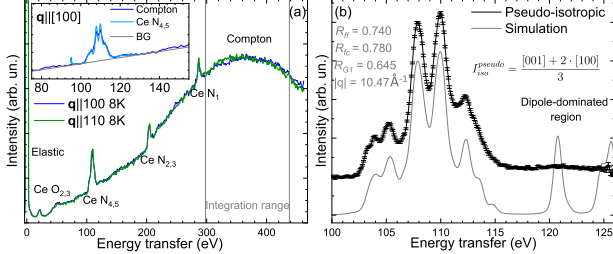


FIG. 8. (a) Experimental NIXS spectra of CeRh₂As₂, displayed in a wider energy window, showing the Compton profile used for normalization and Ce N-edges on top. Linear background correction of the $N_{4,5}$ edge using the wide spectrum, see inset. (b) (Pseudo)isotropic spectrum (black) as constructed from orientation dependent data and optimized simulation (grey). R_{ij} refer to reduction factors and $|q|$ to the momentum transfer in the simulation.

Fig. 9 (a) exhibits the experimental NIXS data and the simulation for $T_K = 0$ K. We show the simulation for the two possible pure $|\Gamma_7\rangle$ ground states that have the same α^2 , i.e. the same charge densities, but different signs of α . The sign refers to a rotation by 45° whereby $\alpha < 0$ stands for lobes along $[110]$ and refers to $|\Gamma_7^-\rangle$. Panel (b) and (c) show the experimental and calculated in-plane difference spectra. The simulation of the difference spectra for the pure $|\Gamma_7\rangle$ states without considering the Kondo effect clearly overestimate the directional dependence but the dichroism of the state with $\alpha < 0$ ($|\Gamma_7^-\rangle$) has the correct sign in the pre-edge [orange lines in (b)]. The contribution of the rotational invariant $|\Gamma_6\rangle$ state and of the highest crystal-field state, the $|\Gamma_7^{\pm}\rangle$ state at 180 K (15.5 meV) with opposite dichroism, reduces the ab -plane anisotropy so that the simulation for the Kondo mixed state with $\alpha < 0$ ($|\Gamma_7^-\rangle$ state) as lowest state fits quantitatively quite well in the pre-edge [red lines in (c)] whereas the assumption of $\alpha > 0$ yields a dichroism with the wrong sign. Also in the interval of 106 to 109 eV the experimental dichroism is positive as is the simulation based on $|\Gamma_7^-\rangle$. For larger energy transfers, the noise due to the increased Compton background (which has been

subtracted) hampers a reliable measurement of the LD.

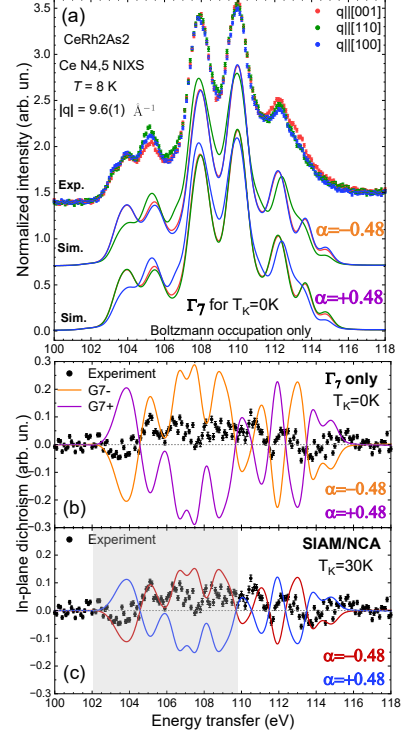


FIG. 9. (a) NIXS directional dependent data with simulations for pure $|\Gamma_7\rangle$ states for $T_K = 0$ K for $\alpha < 0$ and > 0 , and $|\alpha| = 0.48$ giving the amount of $|J_z = \pm 5/2\rangle$ in the ground state. (b)&(c) Experimental ab -plane dichroism $I_{001} - I_{100}$ (black dots). Simulation for $|\Gamma_7\rangle$ states with $\alpha < 0$ and > 0 as in (b) and in the presence of the Kondo effect according to SIAM/NCA calculations in (c).

F. Band structure

A more detailed description of the simple approximation scheme for the Anderson impurity Hamiltonian [45, 46] can be found in Ref. [44] where it was applied to CeCu₂Si₂. It estimates the contributions of the higher lying crystal-field states into ground state.

Also the renormalized band structure calculations [47] in Fig. 10 support the hybridization induced multi-orbital ground state. Here the contributions of the three crystal field states (ground state and excited $4f$ states at 30 and 180 K) are projected out to the respective bands. It turns out that the heavy band at zero energy with mainly $|\Gamma_7^-\rangle$ character has also non-negligible contributions of $|\Gamma_6\rangle$ and $|\Gamma_7^{\pm}\rangle$ states, see Fig. 10.

- [1] J. Flouquet, *Progress in Low Temperature Physics*, edited by W. P. Halperin, Vol. XV (Elsevier, 2005) pp. 139–268, On the Heavy Fermion Road.
- [2] P. Thalmeier and G. Zwicknagl, *Handbook on the Phys. and Chem. of Rare Earths*,

- edited by J.-C. B. K.A. Gschneidner, Jr. and V. Pecharsky, Vol. 34 (Elsevier, 2005) pp. 139–268.
- [3] P. Fulde, P. Thalmeier, and G. Zwicknagl, *Solid State Physics*, edited by H. Ehrenreich and F. Spaepen, Vol. 60 (2006) p. 1, Strongly correlated

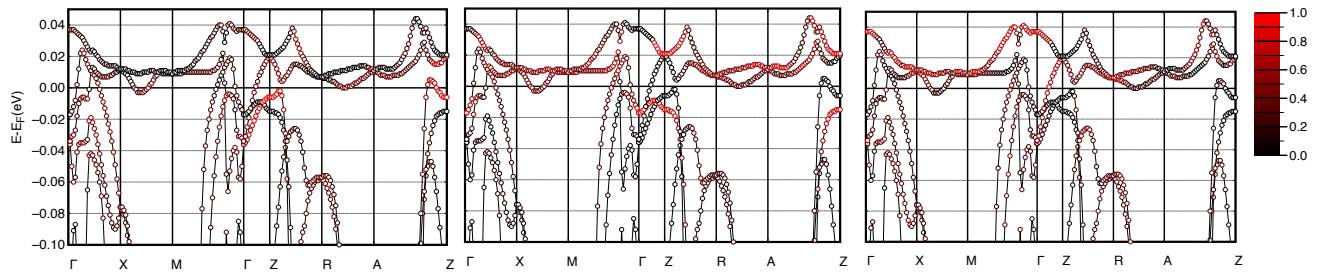


FIG. 10. (left) Renormalized quasiparticle bands, showing the contributions of each crystal-field state; left for $|\Gamma_7^- \rangle$, middle for $|\Gamma_6 \rangle$ and right for $|\Gamma_7^+ \rangle$, red standing for high and black for low occupation.

electrons.

- [4] P. Coleman, *Handbook of Magn. and Adv. Magn. Mater.*, edited by M. F. S. M. H. Kronmüller, S. Parkin and I. Zutic, Vol. 1 (John Wiley and Sons, 2007) pp. 95–148, Heavy Fermions: Electrons at the Edge of Magnetism.
- [5] D. I. Khomskii, *Basic Aspects of the Quantum Theory of Solids* (Cambridge University Press, 2010).
- [6] S. Khim, J. F. Landaeta, J. Banda, N. Bannor, M. Brando, P. M. R. Brydon, D. Hafner, R. Kuchler, R. Cardoso-Gil, U. Stockert, A. P. Mackenzie, D. F. Agterberg, C. Geibel, and E. Hassinger, Field-induced transition within the superconducting state of CeRh_2As_2 , *Science* **373**, 1012 (2021), <https://www.science.org/doi/pdf/10.1126/science.abe7518>.
- [7] S.-i. Kimura, J. Sichelschmidt, and S. Khim, Optical study of the electronic structure of locally noncentrosymmetric CeRh_2As_2 , *Phys. Rev. B* **104**, 245116 (2021).
- [8] M. Kibune, S. Kitagawa, K. Kinjo, S. Ogata, M. Manago, T. Taniguchi, K. Ishida, M. Brando, E. Hassinger, H. Rosner, C. Geibel, and S. Khim, Observation of antiferromagnetic order as odd-parity multipoles inside the superconducting phase in CeRh_2As_2 , *Phys. Rev. Lett.* **128**, 057002 (2022).
- [9] D. Hafner, P. Khanenko, E.-O. Eljaouhari, R. Kuchler, J. Banda, N. Bannor, T. Lühmann, J. F. Landaeta, S. Mishra, I. Sheikin, E. Hassinger, S. Khim, C. Geibel, G. Zwicknagl, and M. Brando, Possible quadrupole density wave in the superconducting Kondo lattice CeRh_2As_2 , *Phys. Rev. X* **12**, 011023 (2022).
- [10] J. F. Landaeta, P. Khanenko, D. C. Cavanagh, C. Geibel, S. Khim, S. Mishra, I. Sheikin, P. M. R. Brydon, D. F. Agterberg, M. Brando, and E. Hassinger, Field-angle dependence reveals odd-parity superconductivity in CeRh_2As_2 , *Phys. Rev. X* **12**, 031001 (2022).
- [11] S. Mishra, Y. Liu, E. D. Bauer, F. Ronning, and S. M. Thomas, Anisotropic magnetotransport properties of the heavy-fermion superconductor CeRh_2As_2 , *Phys. Rev. B* **106**, L140502 (2022).
- [12] D. Möckli and A. Ramires, Two scenarios for superconductivity in CeRh_2As_2 , *Phys. Rev. Research* **3**, 023204 (2021).
- [13] E. G. Schertenleib, M. H. Fischer, and M. Sigrist, Unusual H-T phase diagram of CeRh_2As_2 : The role of staggered noncentrosymmetry, *Phys. Rev. Research* **3**, 023179 (2021).
- [14] A. Ptok, K. J. Kapcia, P. T. Jochym, J. Łażewski, A. M. Oleś, and P. Piekarczyk, Electronic and dynamical properties of CeRh_2As_2 : Role of Rh_2As_2 layers and expected orbital order, *Phys. Rev. B* **104**, L041109 (2021).
- [15] A. Skurativska, M. Sigrist, and M. H. Fischer, Spin response and topology of a staggered-Rashba superconductor, *Phys. Rev. Research* **3**, 033133 (2021).
- [16] K. Nogaki, A. Daido, J. Ishizuka, and Y. Yanase, Topological crystalline superconductivity in locally noncentrosymmetric CeRh_2As_2 , *Phys. Rev. Research* **3**, L032071 (2021).
- [17] D. Möckli and A. Ramires, Superconductivity in disordered locally noncentrosymmetric materials: An application to CeRh_2As_2 , *Phys. Rev. B* **104**, 134517 (2021).
- [18] D. C. Cavanagh, T. Shishidou, M. Weinert, P. M. R. Brydon, and D. F. Agterberg, Nonsymmorphic symmetry and field-driven odd-parity pairing in CeRh_2As_2 , *Phys. Rev. B* **105**, L020505 (2022).
- [19] K. Nogaki and Y. Yanase, Even-odd parity transition in strongly correlated locally noncentrosymmetric superconductors: Application to CeRh_2As_2 , *Phys. Rev. B* **106**, L100504 (2022).
- [20] K. Machida, Violation of Pauli-Clogston limit in the heavy-fermion superconductor CeRh_2As_2 : Duality of itinerant and localized $4f$ electrons, *Phys. Rev. B* **106**, 184509 (2022).
- [21] T. Hazra and P. Coleman, Triplet pairing mechanisms from Hund’s-Kondo models: Applications to UTe_2 and CeRh_2As_2 , *Phys. Rev. Lett.* **130**, 136002 (2023).
- [22] A. Pourret and G. Knebel, Driving multiphase superconductivity, *Science* **373**, 962 (2021), <https://www.science.org/doi/pdf/10.1126/science.abj8193>.
- [23] E. M. Nica, S. Ran, L. Jiao, and Q. Si, Multiple superconducting phases in heavy-fermion metals, *Frontiers in Electronic Materials* **2**, 10.3389/femat.2022.944873 (2022).
- [24] K. Semeniuk, D. Hafner, P. Khanenko, T. Lühmann, J. Banda, J. F. Landaeta, C. Geibel, S. Khim, E. Hassinger, and M. Brando, Decoupling multiphase superconductivity from normal state ordering in CeRh_2As_2 , *Phys. Rev. B* **107**, L220504 (2023).
- [25] J. F. Landaeta, A. M. León, S. Zwickel, T. Lühmann, M. Brando, C. Geibel, E.-O. Eljaouhari, H. Rosner, G. Zwicknagl, E. Hassinger, and S. Khim, Conventional type-II superconductivity in locally noncentrosymmetric LaRh_2As_2 single crystals, *Phys. Rev. B* **106**, 014506 (2022).
- [26] O. Gunnarsson and K. Schönhammer, Electron spectroscopies for Ce compounds in the impurity model, *Phys. Rev. B* **28**, 4315 (1983).
- [27] J. C. Fuggle, F. U. Hillebrecht, Z. Żoźnierek, R. Lässer, C. Freiburg, O. Gunnarsson, and K. Schönhammer, Electronic structure of Ce and its intermetallic compounds, *Phys. Rev. B* **27**, 7330 (1983).
- [28] O. Gunnarsson, K. Schönhammer, J. Allen, K. Karlsson, and O. Jepsen, Information from photoemission spectral weights and shapes, *J. Electron Spectrosc. Relat. Phenom.* **117–118**, 1 (2001).
- [29] M. Sundermann, F. Strigari, T. Willers, J. Weinen, Y. Liao, K.-D. Tsuei, N. Hiraoka, H. Ishii, H. Yamaoka, J. Mizuki, Y. Zekko, E. Bauer, J. Sarrao, J. Thompson, P. Lejay, Y. Muro, K. Yutani, T. Takabatake, A. Tanaka, N. Hollmann, L. Tjeng, and A. Severing, Quantitative study of the f occupation in CeMIn_5 and other cerium compounds with hard x-rays, *J. Elec. Spect. and Rel. Phen.* **209**, 1 (2016).
- [30] T. Willers, D. T. Adroja, B. D. Rainford, Z. Hu, N. Hollmann, P. O. Körner, Y.-Y. Chin, D. Schmitz, H. H. Hsieh, H.-J. Lin, C. T. Chen, E. D. Bauer, J. L. Sarrao, K. J. McClellan, D. Byler, C. Geibel, F. Steglich, H. Aoki, P. Lejay, A. Tanaka, L. H. Tjeng, and A. Severing, Spectroscopic determination of crystal-field levels in CeRh_2Si_2 and CeRu_2Si_2 and of the $4f^0$ contributions in CeM_2Si_2 ($M=\text{Cu, Ru, Rh, Pd, and Au}$), *Phys. Rev. B* **85**, 035117 (2012).
- [31] P. Hansmann, A. Severing, Z. Hu, M. W. Haverkort, C. F. Chang, S. Klein, A. Tanaka, H. H. Hsieh, H.-J. Lin, C. T. Chen, B. Fåk, P. Lejay, and L. H. Tjeng, Determining the crystal-field ground state in rare earth heavy fermion materials using soft-x-ray absorption spectroscopy, *Phys. Rev. Lett.* **100**, 066405 (2008).

- [32] W. Schülke, *Electron Dynamics by Inelastic X-ray Scattering* (Oxford, 2007) Oxford Series on Synchrotron Radiation.
- [33] R. A. Gordon, G. T. Seidler, T. T. Fister, M. W. Haverkort, G. A. Sawatzky, A. Tanaka, and T. K. Sham, High multipole transitions in NIXS: Valence and hybridization in 4f systems, *Europhys. Lett.* **81**, 26004 (2008).
- [34] R. A. Gordon, M. W. Haverkort, S. Sen Gupta, and G. A. Sawatzky, Orientation-dependent x-ray Raman scattering from cubic crystals: Natural linear dichroism in MnO and CeO₂, *J. Phys. Conf. Ser.* **190**, 012047 (2009).
- [35] T. Willers, F. Strigari, N. Hiraoka, Y. Q. Cai, M. W. Haverkort, K.-D. Tsuei, Y. F. Liao, S. Seiro, C. Geibel, F. Steglich, L. H. Tjeng, and A. Severing, Determining the in-plane orientation of the ground-state orbital of CeCu₂Si₂, *Phys. Rev. Lett.* **109**, 046401 (2012).
- [36] M. Sundermann, A. Amorese, F. Strigari, B. Leedahl, L. H. Tjeng, M. W. Haverkort, H. Gretarsson, H. Yavaş, M. M. Sala, E. D. Bauer, P. F. S. Rosa, J. D. Thompson, and A. Severing, Orientation of the ground-state orbital in CeCoIn₅ and CeRhIn₅, *Phys. Rev. B* **99**, 235143 (2019).
- [37] A. Barla, J. Nicolás, D. Cocco, S. M. Valvidares, J. Herrero-Martín, P. Gargiani, J. Moldes, C. Ruget, E. Pellegrin, and S. Ferrer, Design and performance of BOREAS, the beamline for resonant x-ray absorption and scattering experiments at the ALBA synchrotron light source, *J. Synchrotron Rad.* **23**, 1507 (2016), <https://onlinelibrary.wiley.com/doi/pdf/10.1107/S1600577516013061>
- [38] M. Sundermann, K. Chen, H. Yavaş, H. Lee, Z. Fisk, M. W. Haverkort, L. H. Tjeng, and A. Severing, The quartet ground state in CeB₆: An inelastic x-ray scattering study, *Europhys. Lett.* **117**, 17003 (2017).
- [39] J. Weinen, T. Koethe, C. Chang, S. Agrestini, D. Kasinathan, Y. Liao, H. Fujiwara, C. Schüßler-Langeheine, F. Strigari, T. Hauptrecht, G. Panaccione, F. Offi, G. Monaco, S. Huotari, K.-D. Tsuei, and L. Tjeng, Polarization dependent hard x-ray photoemission experiments for solids: Efficiency and limits for unraveling the orbital character of the valence band, *J. Elec. Spect. and Rel. Phen.* **198**, 6 (2015).
- [40] M. W. Haverkort, *Quanta* for core level spectroscopy - excitons, resonances and band excitations in time and frequency domain, *J. Phys. Conf. Ser.* **712**, 012001 (2016).
- [41] R. Cowan, *The Theory of Atomic Structure and Spectra*. (University of California, Berkeley, 1981).
- [42] A. Tanaka and T. Jo, Resonant 3d, 3p and 3s photoemission in transition metal oxides predicted at 2p threshold, *J Phys. Soc. Jpn.* **63**, 2788 (1994).
- [43] M. Sundermann, F. Strigari, T. Willers, H. Winkler, A. Prokofiev, J. M. Ablett, J.-P. Rueff, D. Schmitz, E. Weschke, M. M. Sala, A. Al-Zein, A. Tanaka, M. W. Haverkort, D. Kasinathan, L. H. Tjeng, S. Paschen, and A. Severing, CeRu₄Sn₆: a strongly correlated material with nontrivial topology, *Scientific Reports* **5**, 17937 (2015).
- [44] A. Amorese, A. Marino, M. Sundermann, K. Chen, Z. Hu, T. Willers, F. Choueikani, P. Ohresser, J. Herrero-Martín, S. Agrestini, C. Chen, H.-J. Lin, M. W. Haverkort, S. Seiro, C. Geibel, F. Steglich, L. H. Tjeng, G. Zwicky, and A. Severing, Possible multiorbital ground state in CeCu₂Si₂, *Phys. Rev. B* **102**, 245146 (2020).
- [45] V. Zevin, G. Zwicky, and P. Fulde, Temperature dependence of the 4f quadrupole moment of Yb in YbCu₂Si₂, *Phys. Rev. Lett.* **60**, 2331 (1988).
- [46] G. Zwicky, V. Zevin, and P. Fulde, Simple approximation scheme for the Anderson impurity Hamiltonian, *Z. Phys. B Cond. Matter* **97**, 365 (1990).
- [47] G. Zwicky, Quasi-particles in heavy fermion systems, *Advances in Physics* **41**, 203 (1992), <https://doi.org/10.1080/00018739200101503>.
- [48] M. Sundermann, f-electron charge densities probed using core level non-resonant inelastic x-ray scattering, arXiv preprint arXiv:1911.06901 (2019).